Effect of inelastic scattering on spin entanglement detection through current noise

Pablo San-Jose* and Elsa Prada†
Institut für Theoretische Festkörperphysik, Universität Karlsruhe, 76128 Karlsruhe, Germany
(Dated: May 24, 2019)

We study the effect of inelastic scattering on the spin entanglement detection and discrimination scheme proposed by Egues, Burkard and Loss [Phys. Rev. B 89, 176401 (2002)]. The finite-backscattering beam splitter geometry is supplemented by a phenomenological model for inelastic scattering, the charge-conserving voltage probe model, conveniently generalized to deal with entangled states. We find that the behavior of shot-noise measurements in one of the outgoing leads remains an efficient way to characterize the nature of the non-local spin correlations in the incoming currents for an inelastic scattering probability up to 50%. Higher order cumulants are analyzed, and are found to contain no additional useful information on the spin correlations. The technique we have developed is applicable to a wide range on systems with voltage probes and entanglement.

I. INTRODUCTION

Electron spin has various crucial properties that make it an ideal candidate for a robust carrier of quantum entanglement in solid state systems. Its typical relaxation and dephasing times can be much larger than any other electronic timescale [1, 2], in particular in semiconductor heterostructures, where its controlled manipulation begins to be a reality [3]. This makes electron spin very valuable not only in the context of spintronics [4], but also in the path to a scalable realization of a potential quantum computer.

Moreover, the possibility of demonstrating non-local quantum entanglement of massive particles such as electrons is of conceptual relevance in itself, since it is at the core of the quantum world weirdness. Quantum optics are far ahead in this respect, and present technology can already entangle [5], teleport [6] or otherwise manipulate quantum mechanically [7] the polarization state of photons, and even commercial solutions have been developed [8] for completely secure cryptographic key exchange via optical quantum communication.

In the context of solid state the equivalent feats are far away still, due to the additional difficulties imposed mainly by the fact that massive particles such as electrons suffer from interactions with their environment, which can be in general avoided in the case of photons. This in turn leads to strong decoherence effects, which degrades the entanglement transportation. Sometimes these disruptive effects can be minimized in the case of electron spin with the proper techniques [3]. Still, the problem of controlled spin manipulation and spin detection are two great hurdles to be tackled in the long path to spin-based quantum computation [9]. The main difficulty in the manipulation problem is that all the operations available in usual electronics address electron charge, being completely independent of the electron's spin, unless some additional mechanism involving, e.g., external magnetic fields [4, 10], ferromagnetic materials [11], or spin-orbit coupling [12, 13] are relevant. Such mechanisms usually correlate spin states to charge states, which allows to manipulate and detect the charge states via more conventional means.

Several recent theoretical works have specifically studied the influence of an electromagnetic environment [14, 15, 16] and the decoherence through inelastic processes [17, 18] on orbital and spin-entangled states, such as those that are the subject of the present work. Generally, in all of these cases some type of spin filter was necessary to measure the inequalities, which makes their experimental realization rather challenging.

Another interesting possibility to manipulate and detect spin states with electrostatic voltages is through Pauli blocking, which appears as a spin-dependent 'repulsion' between two electrons due to Pauli exclusion principle, as long as the two electrons share all the remaining quantum numbers. This peculiarity is therefore specific of fermions, and has no analog in quantum optics. An example of the potential of such approach was illustrated in Ref. 19. It relied on the use of the mentioned Pauli blocking mechanism in a perfect four-arm beam splitter supplemented by the bunching (antibunching) behavior expected for symmetric (antisymmetric) spatial two-electron wavefunctions. This was done through the analysis of current noise [19], cross-correlators [20], and Full Counting Statistics (FCS) [21]. It was also shown that it is possible to distinguish between different incoming entangled states [20, 22]. In Ref. 22 it was demonstrated how the shot noise of (charge) current obtained in one of the outgoing leads was enough to measure the precise entangled state coming in through the two input arms, and to distinguish it from a classical statistical mixture of spin states. Finite backscattering and arbitrary mixtures in the spin sector were also considered in Ref. 23, with a focus on the entanglement content and its detection.

In this work we will analyze the robustness of the entanglement detection scheme proposed in Ref. 22 in the presence of spin-conserving inelastic scattering and finite beam-splitter backscattering for various entangled current states. Although the spin sector is not modified by scattering, inelastic scattering changes at least the

*Electronic address: pablo@tfp.uni-karlsruhe.de
†Electronic address: elsa@tfp.uni-karlsruhe.de

energy quantum number of the scattered electrons, and since Pauli exclusion principle does no longer apply to electrons with different energy, we should expect such inelastic processes to degrade the performance of the detection scheme. Moreover, as noted in Ref. 23, the presence of backscattering introduced spurious shot noise that is unrelated to the entanglement of the source. Assuming known backscattering but, in general, unknown inelastic scattering rate we show that the scheme remains valid in certain range of parameter space, and point to a modified data analysis to extract the maximum information out of local shot noise measurements. We further study the information that may be extracted from higher order cumulants of current fluctuations.

We will work within the scattering matrix formalism, and to describe inelastic scattering we will employ a modification of the fictitious voltage probe phenomenological model [24, 25, 26] generalized to include instantaneous current conservation [27] in the presence of entangled states. This approach relies on phenomenological arguments and defines an inelastic scattering probability α that is used to parameterize inelastic effects. Its validity has been widely discussed, in general finding good qualitative agreement with microscopic models [28, 29, 30, 31] and experiments [32], although in certain systems failing at a quantitative level [33]. Recently is was demonstrated to become equivalent to microscopic phase averaging techniques at the Full Counting Statistics (FCS) level in some limits and setups [34]. The scheme remains attractive as a first approximation to inelastic processes. Alternatively, it is a good model for a real infinite-impedance voltage probe, a common component of many mesoscopic devices. The generalization we present here is specifically targeted towards the computation of the FCS of mesoscopic systems with inelastic scattering and incoming scattering states with arbitrary entanglement properties. The problem of how to apply such decoherence model to the particularly interesting case of non-locally entangled input currents has not been previously discussed to the best of our knowledge, except in Ref. 17, where current conservation was not taken fully into account.

This paper is organized as follows. In Sec. II we discuss the beam-splitter device as an entanglement detector in the presence of inelastic scattering. In Sec. III we give a short account of the technique we will employ to compute the FCS. Further details on our implementation of the fictitious probe scheme can be found in Appendix A. The analysis of the obtained results for the operation of the device are explained in Sec. IV. Finally, a summarized conclusion is given in Sec. V.

II. BEAM-SPLITTER DEVICE WITH INELASTIC SCATTERING

The system we will study is depicted in Fig. 1. It is an electronic beam splitter patterned on a two-dimensional electron gas (2DEG) with two incoming and two outgoing arms, such that the transmission probability between the upper and the lower arms is T. The beam splitter is assumed to have also a finite backscattering amplitude whereby electrons get reflected back into the left leads with probability $1-T_B$. We have considered two possibilities for backscattering: the technically simpler case without cross reflection, for which electrons scatter back always into their original incoming leads, and which we will term *simple* backscattering; and the fully symmetric case, whereby the probability of going from any upper lead to any lower lead remains T, be it on the left or the right, which we will call *symmetric* backscattering. This distinction is only relevant when there is a finite inelastic scattering on the leads, and gives otherwise very similar results, so we will focus mainly in the simple backscattering case.

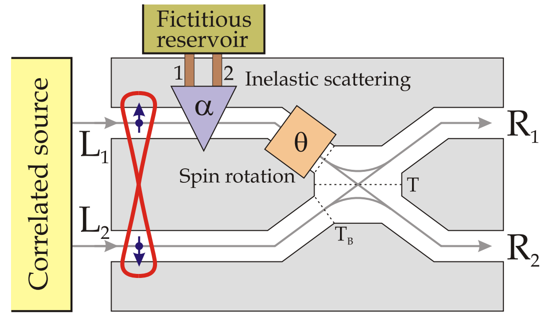

FIG. 1: (Color online) The beam splitter geometry fed with pairwise non-locally entangled electron currents or polarized currents. The action of the spin rotation via Rashba spin-orbit coupling in one of the input leads changes noise in the output leads dramatically. Inelastic transport is modeled between the entangler and the spin rotation region by means of one or more fictitious probes. Shot noise measured in terminal R_1 as a function of θ can be used to detect the nature of the incoming electron correlations.

We connect the right arms to ground and the two incoming arms to a reservoir that emits non-local spin-correlated electron pairs, biased at a voltage $-V$. For definiteness we choose these pairs so that the $\hat{z}$ spin component of the electron coming at a given time through lead L_1 is always opposite to that of the corresponding electron coming simultaneously through lead L_2. They could be or not be entangled, depending on the characteristics of the source and the leads from source to splitter. Time coincidence of pairs is assumed to within a timescale τ_Δ that is shorter than any other timescale in the system, such as $\hbar/V$. If the source is an entangler such as e.g. that of Ref. 35, this would mean that the superconductor emitting the correlated pairs has a large gap Δ as compared to the bias voltage.

A local spin-rotation in lead L_1 is implemented by the addition of backgates above and below a section of lead L_1. Applying a voltage across these backgates the structure inversion asymmetry of the 2DEG is enhanced, inducing a strong Rashba spin-orbit coupling in that region of the 2DEG in a tunable fashion without changing the electron concentration [36]. This in turn gives rise to a precession of the spin around an in-plane axis perpendicular to the electron momentum, which we chose as the $\hat{y}$ axis, resulting in a tunable spin rotation of an angle θ around $\hat{y}$ after crossing the region with backgates.

The idea behind this setup is that the spin rotation can change the symmetry of the spatial part of the electron pair wavefunction, thus affecting the expected shot noise in the outgoing leads, which is enhanced for even and suppressed for odd spatial wavefunctions. The switching from bunching to antibunching signatures in the shot noise as a function of θ is enough to identify truly entangled singlets in the incoming current. Likewise, a θ independent shot noise is an unambiguous signal of a triplet incoming current, since a local rotation of a triplet yields a superposition of triplets, preserving odd spatial symmetry and therefore, antibunching. A current of statistically mixed anticorrelated electron spins can also be distinguished from the entangled cases from the amplitude of the shot noise oscillations with θ. Thus, this device (in the reflectionless case) was proposed as a realizable entanglement detector through local shot noise measurements [22]. The effect of finite backscattering was also analyzed [23], and was found to degrade the performance of the beam-splitter as an entanglement detector.

As discussed in the introduction, inelastic scattering due to environmental fluctuations could spoil the physical mechanism underlying this detector, which is Pauli exclusion principle, and should therefore be expected to affect its performance in some way. The implementation of inelastic scattering in ballistic electron systems can be tackled quite simply on a phenomenological level through the addition of fictitious reservoirs within the scattering matrix formalism [26]. The necessary generalization to deal with entangled currents and a simple scheme to derive the FCS in generic systems with additional fictitious probes is presented in appendix A. We model spin-conserving inelastic scattering by the addition of two fictitious probes (one for spin-up and another for spin-down) in lead L_1, depicted as a single one in Fig. 1. We have numerically checked that the addition of another two fictitious probes in lead L_2 gives very similar results for the shot noise through the system, so we will take only two in the upper arm for simplicity. This is also physically reasonable if we consider only decoherence due to the backgates deposited on the upper arm to perform the local Rashba spin-rotation, which provide a large bath of external fluctuations that can provide much more effective inelastic scattering. The parameter that controls the inelastic scattering probability is $\alpha \in [0, 1]$, being $\alpha = 1$ the completely incoherent limit. For a discussion of the effect of spin dephasing in elastic transport see Refs. 23, 37, 38.

In the following analysis we will inject into the input arms of the device currents with different types of initial non-local electron-pair density matrix,

$$\hat{\rho} = \frac{1}{2}\left(|L_1\!\uparrow; L_2\!\downarrow\rangle\langle L_1\!\uparrow; L_2\!\downarrow| + |L_1\!\downarrow; L_2\!\uparrow\rangle\langle L_1\!\downarrow; L_2\!\uparrow|\right) + \frac{\beta}{2}\left(|L_1\!\downarrow; L_2\!\uparrow\rangle\langle L_1\!\uparrow; L_2\!\downarrow| + |L_1\!\uparrow; L_2\!\downarrow\rangle\langle L_1\!\downarrow; L_2\!\uparrow|\right), \quad (1)$$

namely, i) statistical mixtures of up and down classically correlated electrons (diagonal density matrix, $\beta = 0$), which we will also call spin-polarized currents, ii) EPR-type singlet spin-entangled pure states ($\beta = -1$), and iii) idem with $m_s = 0$ triplet states ($\beta = 1$). We will use subindexes s, t, and m to denote the pure singlet, pure $m_s = 0$ triplet and statistically mixed incoming states.

Our goal is to ascertain to what extent, for a splitter transmission T, a finite backscattering $1 - T_B$ and finite and unknown amount of inelastic scattering α in the input leads, the shot noise in one of the output arms (R_1) as a function of rotation angle θ could still be used to demonstrate the existence or not of initial entanglement, and that way provide a means to distinguish truly quantum-correlated states from statistically correlated ones (unentangled).

III. THE TECHNIQUE

In Appendix A we give a detailed account of the method we have used, which can be employed to compute the FCS of a generic mesoscopic conductor with instantaneous current conservation in the attached voltage probes, and quantum entanglement in the incoming currents. A sequential scattering approximation is implicit, which however yields the correct $\omega = 0$ current fluctuations in known cases. We summarize here the main points as a general recipe for practical calculations.

Given a certain mesoscopic system with a number of biased external leads connected to reservoirs, one should add the desired voltage probes to model inelastic scattering (or real probes), and perform the following steps to compute the long-time FCS of the system:

(i) Define the (possibly entangled) incoming states in the external leads for a single scattering event without the probes,

$$|in\rangle = R[\{\hat{a}^+\}]|vac\rangle. \quad (2)$$

Here $R[\{\hat{a}^+\}]$ is an arbitrary combination of creation operators a_k^+ of incoming electrons acting on the system's vacuum.

(ii) Add the N two-legged voltage probes with individual scattering matrices as in Eq.. (A1), and compute the total S-matrix of the multi-terminal system, S_{lk}.

(iii) Define outgoing electron operators $\hat{b}_j^+ = \sum_k S_{lk}\hat{a}_k^+$. To implement instantaneous current conservation we expand our Hilbert space with N integer slave degrees of freedom $\vec{Q} = \{Q_i\}$, which result in the following outgoing state after one scattering event,

$$|out;\vec{Q}\rangle \equiv R[\{\hat{b}^+\}]\prod_i^N\left[\hat{b}^+_{p_i;1}\hat{b}^+_{p_i;2}\right]^{g(Q_j)}|vac\rangle. \quad (3)$$

These Q_i are quantum counters of total charge accumulated in the probes. The notation here is that $\hat{b}^+_{p_i;n}$ creates the scattered state resulting from an electron injected through leg n of the two-legged probe i. $g(Q)$ encodes the response of the probe to a certain accumulated charge Q. The choice given in Eq.. (A15) yields in our setup a tripled-valued fluctuation interval of $Q_i \in [-1, 1]$. Note also that state $|out;\vec{Q}\rangle$ in the above equation is nothing but $U_{\Delta t}|\phi^e_j\vec{Q}\rangle$ of Appendix A.

(iv) Compute the $3^N \times 3^N$ $\overline{W}$ matrix

$$\overline{W}_{\vec{Q}_b\vec{Q}_a}(\vec{\lambda}) = \langle out;\vec{Q}_1|\hat{P}_{\vec{Q}_2}\hat{\chi}(\vec{\lambda})|out;\vec{\bar{Q}}_1\rangle, \quad (4)$$

which we write in terms of the moment generating operator $\hat{\chi} = e^{i\sum_k \lambda_k(\hat{N}^{\rm out}_k - \hat{N}^{\rm in}_k)}$. The operator $\hat{P}_{\vec{Q}_2}$ projects onto the subspace of electron states that have a total of $Q_{2_i} - g(Q_{1_i})$ particles scattered into probe i, i.e., states in which the probe i has gone from Q_{1_i} to Q_{2_i} excess electrons. If the incoming state is not a pure state, one should perform the statistical averaging over the relevant $|out;\vec{Q}\rangle$ states at this point.

(v) Compute the resulting long-time *current* moment generating function $\chi_I(\vec{\lambda})$ by taking the maximum eigenvalue of matrix $\overline{W}$. The charge generating function $\chi(\vec{\lambda})$ is obtained simply by multiplying the current one by $M = eVt/h$, where M is the average number of emitted pairs from the source after an experiment time t at a bias V.

We make use of this method in our particular system by setting a single counting field λ on output lead $R1$, where we wish to compute current fluctuations. This way we derive results for χ_I and current cumulants [see Eqs.. (A17) and (A18)] from the corresponding $\overline{W}$ matrix (4) for the different types of injected currents of Eq. (1).

While explicit expressions for the current cumulant generating function $\log\chi_I(\lambda)$ are in general impossible due to the large dimensions of the $\overline{W}$ matrix (9×9 in this case), it is always possible to write χ_I in an implicit form that is just as useful to sequentially compute all cumulants, namely the eigenvalue equation

$$\det\left[\overline{W}(\lambda) - \chi_I(\lambda)\mathbf{1}\right] = 0, \quad (5)$$

supplemented by the condition $\chi_I(0) = 1$. By differentiating this equation around $\lambda = 0$ a number of times and using (A17) one can obtain the various zero-frequency current cumulants on arm $R1$.

In the next section, instead of giving the general expression of $\overline{W}$, which is rather large, we provide the explicit expressions for χ_I and shot noise obtained in various useful limiting cases, together with plots of the first cumulants in the $\{T, T_B, \alpha, \theta\}$ parameter space.

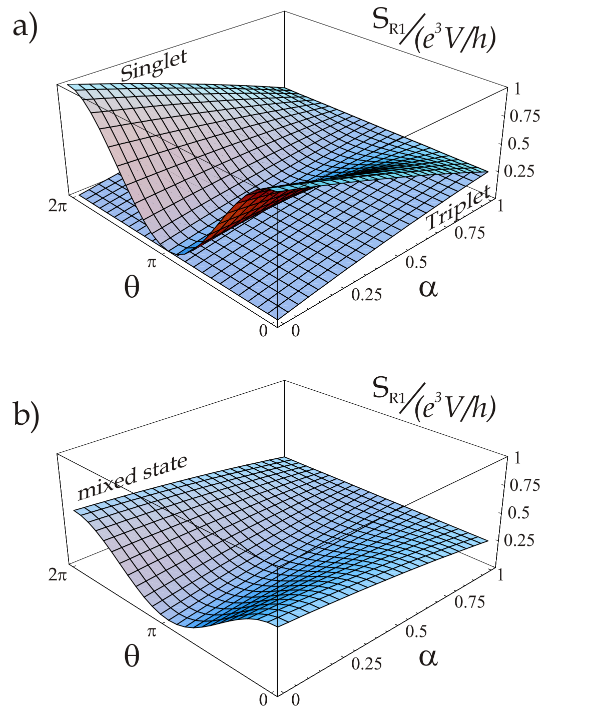

FIG. 2: (Color online) In the upper plot (a) we represent the current shot-noise in units of e^3V/h in lead $R1$ for the singlet and $m_s = 0$ triplet incoming states, as a function of spin rotation angle θ and decoherence strength α. The same for the polarized spin state case is presented in the lower plot (b). Inter-lead transmission probability between upper and lower arms T is fixed to 0.5, and no backscattering ($T_B = 1$) is assumed.

IV. RESULTS

In this section we will analyze the performance of the beam splitter device of Fig. 1 as a detector of quantum correlations in the incoming currents through the shot noise or higher current cumulants induced in arm R_1. We will first make connection with the results in the literature [22] by computing the shot noise in an elastic splitter, and then we will generalize them to finite inelastic scattering probabilities and finite backscattering. We will thus establish tolerance bounds for such imperfections in the detector. Finally, we will address the question of whether the measurement of higher order current cumulants could improve the tolerance bounds of the device.

A. Shot noise

In the elastic transport limit $\alpha = 0$ and with arbitrary intralead backscattering strength $1 - T_B$, the following expression for the shot noise is obtained,

$$S = \frac{e^3|V|}{h} T_B \left[1 - T_B + (1-\beta) T_B T(1-T)(1+\cos\theta)\right], \tag{6}$$

where constant β corresponds to the different types of incoming current, cf. Eq. (1). Note that this expression holds for simple or symmetric backscattering (as defined in Sec. II). As shown by Eq. (6), for $\alpha = 0$ the amplitude of the θ dependence is enough to distinguish between the different types of states, if T and T_B are known. As could have been expected, the triplet current noise ($\beta = 1$) is θ independent, since the local spin rotation only transforms the $m_s = 0$ triplet to a different superposition of the other triplet states, none of which can contribute to noise since each electron can only scatter into different outgoing leads due to the Pauli exclusion principle.

However, in the presence of a strong coupling to the environment, $\alpha = 1$, the shot noise behaves very differently. Due to the complete incoherence of scattering, which changes the orbital quantum numbers of the incoming states, the bunching-antibunching switching disappears. Therefore S_s, S_t and S_m become equal and θ independent. In particular, for simple backscattering we have

$$S_s = S_t = S_m = \frac{e^3|V|}{h} \frac{T_B}{(1+T_B)^3} \left[1 + 2T_B^2 T(1-T) - T_B(1+3T^2-6T) - T_B^3 T^2 (2+T_B)\right]. \tag{7}$$

These features are illustrated for $T_B = 1$ and $T = 1/2$ in Fig. 2, where we have plotted the current shot-noise in lead R_1, normalized to the constant e^3V/h [45], as a function of the spin rotation angle θ and the decoherence parameter α. Note that for $\alpha = 1$ (and without backscattering), Eq. (7) reduces to $S_s = S_t = S_m = (e^3V/h)T(1-T)$, which is 1/4 in normalized units. The cosine-type dependence of the current noise with θ, $S(\theta) = S(\pi) + \Delta S \cos^2(\theta/2)$, where $\Delta S = S(\theta = 0) - S(\theta = \pi)$, holds for any value of $\alpha < 1$ in the singlet and polarized cases. The oscillation amplitude of the noise for the singlet case is always twice the oscillation amplitude of the polarized one. In contrast, the triplet shot noise (and all higher cumulants for that matter) remains always θ independent for any α and T_B.

Since our aim in this study is to find a way to distinguish between the different incoming states of Eq. (1), we will disregard from now on the trivial case of the triplet current, which is easily detectable by its θ-independence, and focus entirely on the distinction between the singlet and mixed state cases. In these two cases, when $T_B < 1$, the oscillatory behavior with θ remains, although it is no longer purely sinusoidal. Besides, its oscillation amplitude quickly decreases, making the entanglement detection scheme harder. However, we will now show that, knowing only the value of the shot-noise at zero spin rotation angle (or alternatively the amplitude ΔS), it is possible to distinguish between the different incoming states for not-too-strong decoherence.

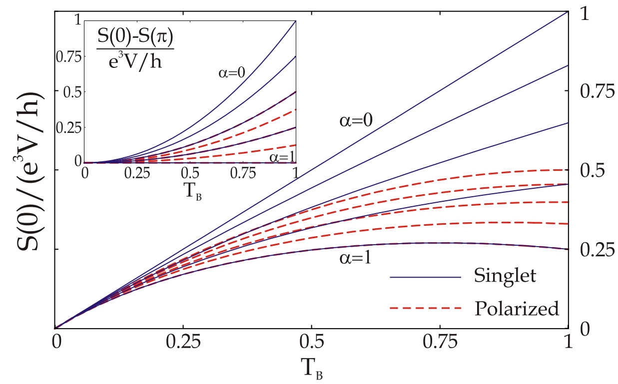

FIG. 3: (Color online) Normalized value of shot-noise in lead R_1 at zero spin rotation angle as a function of beam splitter transmission T_B for $T = 0.5$. Straight (blue) lines correspond to singlet incoming current whereas dashed (red) lines account for the polarized one. In both cases, different values of inelastic scattering probability have been considered, from $\alpha = 0$ (upper curves) to $\alpha = 1$ (lower curves) in steps of 0.25. Inset: the same for the oscillation amplitude with θ of the shot-noise.

B. Robust entanglement detection scheme

Tuning once again the beam splitter to the symmetric $T = 1/2$ point, which turns out to be the optimum point of operation for entanglement detection, we notice from Fig. 2 that the analysis of the θ dependence of the shot-noise at an arbitrary and unknown value of α indeed precludes from a clear distinction of the singlet and mixed state cases.

A more complete picture can be obtained by plotting the value of the shot-noise at $\theta = 0$ in the interval $\alpha \in [0, 1]$ as a function of T_B. This is done in Fig. 3 for the case of simple backscattering. Solid (blue) lines correspond to singlet incoming current, and dashed (red) lines to the polarized one. Moreover, the upper curve in both sets of curves accounts for the case of $\alpha = 0$, and for the next ones the value of the inelastic scattering parameter increases, in steps of 0.25, until $\alpha = 1$ for the lower curves (which coincide for both the entangled and polarized cases). The same analysis can be than for the behavior of the amplitude ΔS as a function of T_B, as shown in the inset of Fig. 3 (given also for simple backscattering). In this case, the amplitudes for both the singlet and the polarized currents have in fact a very simple analytical form, the singlet case ranging from T_B^2 to 0 and the polarized one from $T_B^2/2$ to 0 as we sweep from $\alpha = 0$ to $\alpha = 1$. Therefore, we see how the θ-independent background noise introduced by the finite backscattering,in the main plot of Fig. 3, which could in principle degrade the performance of the entanglement detector as mentioned in Ref. 23, can be filtered out by measuring the amplitude ΔS. We also note that if a symmetric backscattering is considered, the resulting curves for Fig. 3 are qualitatively the same, and therefore does not affect the above discussion.

We can observe in both plots of Fig. 3 that if α is unknown, as it is usually the case in an experiment, the classical and quantum currents are distinguishable from a single noise measurement (or two in the case of the inset) only if its value is found to lie outside of the overlapping region between the two sets of curves. According to this model, this should always happen for values of inelastic scattering smaller than at least one half. In the case of the main figure, even higher values of α can be distinguished for values of T_B close to one. In any case, the values of α for which the noise measurement is no longer able to distinguish a singlet entanglement from a statistically mixed case are rather high, $\alpha \in [0.5, 1]$. This means that, in a realistic situation where decoherence is not too high, shot-noise measurements remain enough for determining if the source feeding the beam-splitter is emitting entangled or statistically mixed states.

C. Higher order cumulants

We could ask whether it is possible to distinguish between incoming singlet-entangled and polarized currents for a wider range of parameters α by analyzing higher order cumulants. The short answer is 'no'.

As we did for the noise in Fig. 2, we can plot the angular dependence of the third moment, the skewness, for different values of inelastic scattering parameter α. This is shown in a 2D plot in the inset of Fig. 4(b) for $T = 0.5$ and $T_B = 1$. As before, solid (blue) lines and dashed (red) lines correspond to spin singlet-entangled and polarized incoming currents, respectively. Now we find that the behavior of skewness with θ is not monotonous as α varies. For $\alpha = 0$ and for $\alpha = 1$ at $T_B = 1$ the third cumulant is zero for every angle both for entangled and for mixed states (the probability distribution of the current is symmetric for those parameters as was previously noted in the $\alpha = 0$ case in Ref. [21]). Moreover, this means that the skewness is not a good entanglement detector for a near perfect beam splitter, nor when the inelastic scattering in strong. For intermediate values of decoherence, still at $T_B = 1$, the skewness oscillates with the spin rotation angle and its oscillation amplitude, $\langle\langle I^3\rangle\rangle(\theta = 0) - \langle\langle I^3\rangle\rangle(\theta = \pi)$, has a maximum around $\alpha \approx 0.5$. This oscillation range is depicted in the main plots of Fig. 4 as a function of the transmission between left and right arms T_B (where simple backscattering has been considered). Several values of the inelastic parameter are differentiated using different shades of grey, ranging from pale gray for $\alpha = 0$ to dark gray for $\alpha = 1$ in steps of 0.25. The main features can be summarized as follows. First, both for the entangled and the polarized current, the broadest oscillation range occurs for $\alpha = 0$ (being bigger for the singlet-entangled case). Second, for $\alpha = 1$ the oscillation amplitude in both cases is zero, although the skewness remains finite and positive (shifting from a Gaussian to a Poissonian distribution of current as T_B goes from 1 to 0). For T_B smaller than 0.9 approximately, the behavior of the oscillation range is monotonous with α, it simply decreases with it. For small values of T_B, the skewness coincides with the shot-noise, which is expected since the probability distribution for a tunnel barrier recovers a Poisson distribution, even in the presence of inelastic scattering. In general, the sign of the skewness is reversed in a wide range of parameters by tuning the spin rotation θ.

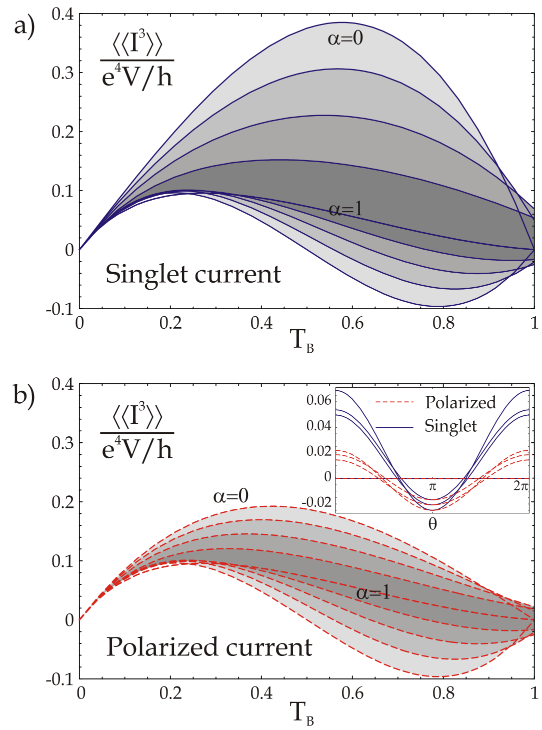

FIG. 4: (Color online) Oscillation range with angle θ of the skewness in lead R_1, in units of e^4V/h, as a function of beam-splitter transmission between left and right arms T_B. T is fixed to the optimal point $T = 0.5$. Different oscillation ranges for different values of inelastic scattering are indicated by different shades of grey, ranging from pale gray for $\alpha = 0$ to dark gray for $\alpha = 1$ in steps of 0.25. The case of singlet-entangled incoming current is considered in plot (a), whereas in plot (b) the incoming current is in a polarized state. The actual oscillation of skewness with Rashba spin rotation angle for entangled current (solid blue lines) and polarized current (dash red lines) is plotted in the inset of figure (b).

Concerning our entanglement detection motivation, comparing Fig. 4(a) and 4(b) we find that the third cumulant doesn't provide any further information in our search of a way to distinguish between entangled and non-entangled incoming states. For T_B of the order of 0.9 and above, due to the non-monotonous behavior of the oscillation range with α, the skewness of our beam splitter setup can hardly be used as a detector on entanglement at all. For smaller values of T_B, we are able to discriminate between different currents in the same range of inelastic scattering parameter α as we could with the noise, this is, from zero decoherence to roughly $\alpha = 0.5$.

We have also analyzed further cumulants, whose behaviors with T_B and θ get more intricate as the order of the cumulant increases, and have found the same qualitative result. Either they are not useful tools for entanglement detection or the range of parameters α and T_B is not improved from what we find with the shot-noise measurements.

V. CONCLUSIONS

In this work we have analyzed the effect of inelastic scattering, modeled by spin-current conserving voltage probes, on entanglement detection through a beam-splitter geometry. We have shown that, unlike elastic orbital dephasing [37], the action of inelastic processes in the beam-splitter cannot be neglected, since it directly affects the underlying physical mechanism of the detector, which is the fact that two electrons with equal quantum numbers cannot be scattered into the same quantum channel. If energy is not conserved, such antibunching mechanism is no longer perfect, and the entanglement detection scheme has to be revised.

However, we have found that the detection of entanglement through shot noise measurements remains possible even under very relaxed conditions for imperfections in the beam-splitter device and substantial inelastic scattering. Even if a reliable microscopic description of inelastic processes is not available, the present analysis suggests that the detection scheme is robust for inelastic scattering probabilities up to 50%.

We have also shown that higher current cumulants do not contain more information about the entanglement of the incoming currents than the shot noise. We have analyzed in particular the skewness of current fluctuations, finding that finite backscattering and inelastic scattering strongly affect the asymmetry of current fluctuations, but specially so in the singlet entangled case, where a positive skewness is developed as the beam splitter transparency is lowered.

Finally, we have developed a novel way to implement current conservation in voltage probe setups when the incoming currents are non-locally entangled, which can be applied to a wide variety of problems where entanglement is key.

Acknowledgments

We would like to acknowledge the inspiring conversation with M. Büttiker that encouraged us to develop our formulation of the voltage probe FCS with entanglement. We also enjoyed fruitful discussions with D. Bagrets, F. Taddei, R. Fazio and C.W.J Beenakker. This work benefited from the financial support of the European Community under a Marie Curie Research Training Network, and the SQUBIT2 project, number IST-2001-39083.

APPENDIX A: PHENOMENOLOGICAL DESCRIPTION OF INELASTIC SCATTERING

Voltage probes are frequently real components of mesoscopic devices, but have also been used traditionally for phenomenological modeling purposes. The voltage probe description of inelastic scattering resorts to the addition of one or more fictitious reservoirs and leads attached to the coherent conductor under study through specific scattering matrices, around the regions where inelastic scattering is to be modeled. While being still coherent overall, the elimination of the fictitious reservoirs results in an effective description of transport such that electrons that originally scattered into the reservoirs now appear as having lost phase and energy memory completely.

We will now discuss the implementation of the voltage probe in the presence of charge relaxation and general incoming states. The whole idea of the voltage probe is to use the non-interacting scattering formalism to model inelastic electron scattering, and the crossover from coherent conductors to incoherent ones. There are two ways to do this. The simpler one assumes a static chemical potential in the probes that is computed self-consistently by fixing time-averaged current flowing into the probes to zero, as corresponds to an infinite impedance voltage probe, or to inelastic scattering. This gives a physically sound conductance value, but fails to yield reasonable shot noise predictions. The reason is that total current throughout the system should be instantaneously conserved. The more elaborate way, therefore, assumes fluctuations in the state of the probe that can compensate the current flowing into the probe(s) at any instant of time (and possibly also energy if one is modeling pure elastic dephasing [39, 40, 41]), which gives results for current fluctuations in agreement with classical arguments [26].

It is traditional to impose such constraint within a Langevin description of current fluctuations [27], whereby the chemical potential in the probe is allowed to fluctuate, but the semiclassical character of this approach makes it inadequate to treat the statistics of general incoming entangled states. The discussion to follow (and the implicit sequential scattering approximation) doesn't rely on a defined stochastic chemical potential, but can be shown to yield completely equivalent results to the Langevin approach in the case of non-entangled incoming states, and does not suffer from such shortcoming.

The scattering matrix to a (two-legged) fictitious probe is given, in the bases $1, 2, 1', 2'$ (being $1', 2'$ the extra leads), by

$$S_\alpha = \begin{pmatrix} 0 & -\sqrt{1-\alpha} & i\sqrt{\alpha} & 0 \\ \sqrt{1-\alpha} & 0 & 0 & i\sqrt{\alpha} \\ i\sqrt{\alpha} & 0 & 0 & \sqrt{1-\alpha} \\ 0 & i\sqrt{\alpha} & -\sqrt{1-\alpha} & 0 \end{pmatrix}, \tag{A1}$$

with α being the inelastic scattering probability. This should be composed together with any other scattering matrices in the system, and any other probes present. In a spinful case in which inelastic scattering does not flip spin there should be at least two of these probes, one per spin channel. Other considerations such as inelastic channel mixing in multichannel cases should be taken into account when designing the relevant fictitious probe setup. Let us first consider a general setup with a single probe for simplicity.

We will now introduce the implementation of charge conservation through the system (i.e. in the fictitious probe) which will lead to the simple result expressed in Eq. (A16). We first make the essential approximation that the inelastic scattering time in the interacting region is much smaller than

$$\Delta t \equiv h/eV. \tag{A2}$$

The inverse of the timescale Δt is the average rate at which the external leads inject particles into the system, in the localized wave-packet terminology [42]. We will call the scattering processes within time interval Δt a 'scattering event'. In this limit of quick scattering we can assume *sequential* scattering events, as if each Δt interval was an independent few-particle scattering problem, one for each time

$$t_j \equiv j\Delta t. \tag{A3}$$

The overlap of the wave-packets which would in principle give contributions away from the sequential scattering approximation was shown to have a negligible effect in the long time limit [43]. Furthermore, if one considers small transparency contacts between the electron source and the fictitious probes, the sequential scattering approximation is also exact.

The incoming state in each scattering event will be one particle in each channel of the external leads (L_1 and L_2 in the setup of Fig. 1), plus a certain state in the probe's leads $1'$ and $2'$. This probe incoming state is prepared in a way so as to compensate for excess charge scattered into the fictitious probe in all previous events, with the intention of canceling any current that has flowed into the probe in the past. The book-keeping of the probe's excess charge is done via an auxiliary slave degree of freedom $|Q\rangle$ with discrete quantum numbers $Q = 0, \pm1, \pm2, \dots$ that count charge transferred to the probe. The incoming state in leads $1'$ and $2'$ injected by the probe into the system is a function of Q. The time evolution of slave state $|Q\rangle$ is constrained so that Q always equals the total number of electrons that has entered the probe since the first scattering event. In particular the time evolution of $|Q\rangle$ during one scattering event Δt is taken to follow the resulting net charge that was transferred to the probe during that event. This scheme effectively correlates the initially uncorrelated scattering events in order to given instantaneous current conservation through the system.

If the incoming state in the probe's leads is chosen correctly the number of Q states between which $|Q\rangle$ will fluctuate during many scattering events will be bounded, and will be independent of the total number of events

$$M = eVt/h \tag{A4}$$

in the total experiment time t. This is the underlying principle of this approach, which will guarantee that the instantaneous charge fluctuations in the probe will be bounded to a few electrons throughout the whole measurement process, i.e. the probe current will be zero and noiseless at frequencies below $eV/\hbar$.

The choice that minimizes the charge fluctuations in a single channel two-legged probe in the absence of superconductors in the system is the following: if Q at the beginning of the scattering event is 1 or 2, the probe will emit two particles, one through each 'leg', thereby losing a maximum of 2 and a minimum of 0 in that event; if Q is 0, -1 or -2 the probe will not emit any particle, thereby absorbing a maximum of 2 and a minimum of 0. The resulting fluctuations of Q are bounded in the $[-2, 2]$ range. In some cases, such as the system discussed in the main text, this range is reduced to $[-1, 1]$ owing to the fact that for $Q \le 0$ the probe will never absorb 2 particles, but a maximum of 1. The relevance of this discussion will be apparent in connection with Eq. (A11), since it will determine the dimensions of the W operator therein.

1. Sequential scattering scheme for the Full Counting Statistics

We wish to compute in a general case the characteristic function

$$\chi(\vec{\lambda}; M) = \langle e^{i\sum_k \lambda_k \Delta\hat{N}_k}\rangle = \mathbf{Tr}\left\{\hat{\chi}(\vec{\lambda})\rho(t)\right\} \tag{A5}$$

after a total measuring time interval t. Number difference $\Delta\hat{N}_k \equiv \hat{N}_k^{\rm out} - \hat{N}_k^{\rm in}$ is defined as the number operator at time t (scattered outgoing particle number) minus the number operator at time zero, before any scattering (incoming particle number). Differentiating $\log\chi$ respect to the counting fields λ_k one obtains the different transferred charge and current cumulants, Eq. (A17).

Let us include the fictitious probe and expand our Fock space with the slave degree of freedom $|Q\rangle$. We take the density matrix of the whole system at time zero equal to $\rho(0) = \rho^Q(0)\otimes\rho^e(0)$, the second ρ being the electronic density matrix. As we will see we do not need to specify the initial state of the slave degree of freedom $\rho^Q(0)$ since it will not affect our results in the long time limit. The density matrix is factorized in the localized wave-packet basis [42],

$$\rho(0) = \rho^Q(0)\otimes\prod_j^{\otimes}\rho_j^e, \tag{A6}$$

with the electronic part being $\rho_j^e \equiv \rho_j^r\otimes\rho_j^p$. Each of these ρ_j^e constitutes the incoming state in each of the j scattering events corresponding to the time interval $[t_j, t_{j+1}]$.

ρ^r_j, which is actually j-independent, is the density matrix of the (uncorrelated) electrons coming from the external reservoirs, and ρ^p_j is the density matrix of the (correlated-through-Q) electrons coming from the fictitious probe. As we mentioned, this matrix ρ^p_j will depend on the state of the slave degree of freedom Q at the beginning of each scattering event j.

The time evolution from 0 to t, $\rho(t) = \hat{U}_t\rho(0)\hat{U}_t^+$ is split up in the M time intervals of length Δt. The sequential scattering approximation amounts to assuming that in each event each electron group ρ^e_j scatters completely before the next one does. Therefore $\hat{U}_t = \hat{U}^M_{\Delta t}$. We defer the discussion on how precisely $U_{\Delta t}$ operates to a little later.

Since operator $\hat{\chi}(\vec{\lambda})$ will factorize into contributions for each scattering event, $\hat{\chi} = \prod_j \hat{\chi}_j$, we can rewrite equation (A5) as

$$\begin{aligned}\chi &= \mathbf{Tr}_Q\left\{\mathbf{Tr}_M\left[\hat{\chi}_M U_{\Delta t}\rho^e_M \mathbf{Tr}_{M-1}\left[\ \cdots\right.\right.\right. \\ &\cdots\ \left.\left.\left.\mathbf{Tr}_1\left[\hat{\chi}_1 U_{\Delta t}\rho^e_1\rho^Q(0)U^+_{\Delta t}\right]U^+_{\Delta t}\right]U^+_{\Delta t}\cdots\right]\right\},\end{aligned} \tag{A7}$$

where $\mathbf{Tr}_j$ stands for the trace over the ρ^e_j electron states and $\mathbf{Tr}_Q$ over the Q subspace. An alternative way of writing this is by induction. Defining an auxiliary operator $\hat{\Phi}^{(k)} = \sum_{QQ'}|Q\rangle\Phi^{(k)}_{QQ'}\langle Q'|$ such that

$$\hat{\Phi}^{(j)} = \mathbf{Tr}_j\left[\hat{\chi}_j U_{\Delta t}\rho^e_j\hat{\Phi}^{(j-1)}U^+_{\Delta t}\right], \tag{A8}$$

$$\hat{\Phi}^{(0)} = \rho^Q(0), \tag{A9}$$

one can see that (A7) and (A5) are equivalent to

$$\chi(\vec{\lambda};M) = \mathbf{Tr}_Q\hat{\Phi}^{(M)}. \tag{A10}$$

After some algebra, Eq. (A8) can be recast into the following sum over the total range of Q values,

$$\Phi^{(j)}_{Q_bQ'_b} = \sum_{Q_aQ'_a} W^{Q_aQ'_a}_{Q_bQ'_b}\Phi^{(j-1)}_{Q_aQ'_a}, \tag{A11}$$

with the W superoperator

$$W^{Q_aQ'_a}_{Q_bQ'_b}(\vec{\lambda}) = \mathbf{Tr}_j\left[P_{Q'_bQ_b}\hat{\chi}_j(\vec{\lambda})U_{\Delta t}\rho^e_j P_{Q_aQ'_a}U^+_{\Delta t}\right], \tag{A12}$$

and $P_{QQ'} \equiv |Q\rangle\langle Q'|$ the generalized projector within the slave degree of freedom space. We will specify how it operates in practice a bit later, after Eq. (A14).

Some words about the meaning of this operator W, which is a central object in this technique, are in order at this point. It is a superoperator that, for $\vec{\lambda}=0$ simply transforms the reduced density matrix $\rho^Q(t_j) = \hat{\Phi}^{(j)}(\vec{\lambda}=0)$ of the slave degree of freedom at time t_j to the subsequent one $\hat{\Phi}^{(j+1)}(\vec{\lambda}=0)$ at time t_{j+1}. In Eq. (A8) we see how $\hat{\Phi}^{(j)}$ is simply $\hat{\Phi}^{(j-1)}$ to which the incoming state ρ^e_j for event j is added, is allowed to evolve a time Δt (during which also ρ^Q evolves as dictated by the number of electrons scattered into the probe), and the scattered electrons are traced out. The result is the new evolved reduced density matrix for the slave degree of freedom. For finite $\vec{\lambda}$ the corresponding counting fields for the scattered electrons are also included into $\hat{\Phi}^{(j)}$ to be able to recover the desired cumulants of the traced-out electrons after time t from $\chi = \mathbf{Tr}_Q\hat{\Phi}^{(M)}$. This can be also seen as supplementing the dynamics of the system with a quantum field term $\propto \lambda_k$ in the action, in the generalized Keldysh language of Ref. 44.

By assuming without loss of generality a diagonal initial $\rho^Q(0)$ and by noting that by construction states with different Q are orthogonal, we can in general take W to be diagonal $W^{Q_aQ'_a}_{Q_bQ'_b} = \delta_{Q_aQ'_a}\delta_{Q_bQ'_b}\overline{W}_{Q_bQ_a}$, and $\Phi^{(j)}_{QQ'} = \delta_{QQ'}\Phi^{(j)}_Q$. Therefore (A10) finally becomes

$$\chi(\vec{\lambda};M) = \sum_{Q_1Q_2}\overline{W}^M_{Q_1Q_2}\rho^Q_{Q_2Q_2}(0) \tag{A13}$$

(note the M^{th} power of the $\overline{W}$ matrix). The following alternative and useful form for (A12) can be obtained by writing $|Q\rangle\langle Q|\rho^e_j|Q\rangle\langle Q| = |\phi^eQ\rangle\langle\phi^eQ|$, in the case of a pure incoming state in the external leads,

$$\overline{W}_{Q_bQ_a}(\vec{\lambda}) = \langle\phi^eQ_a|U^+_{\Delta t}P_{Q_bQ_b}\hat{\chi}_j(\vec{\lambda})U_{\Delta t}|\phi^eQ_a\rangle, \tag{A14}$$

where $|\phi^eQ\rangle$ stands now for the incoming electronic state (through all leads) that corresponds to a given value Q of the slave degree of freedom.

Let us analyze the action of the evolution operator $U_{\Delta t}$ in the above equation. Since we assume that particles scatter fully in time Δt, the action of $U_{\Delta t}$ on the electrons is written in terms of the global scattering matrix, $b^+_k = U_{\Delta t}a^+_kU^+_{\Delta t} = S_{kl}a^+_l$, where a^+_k are the electron creation operators in the different leads (including fictitious ones) of the system [46]. The effect of $U_{\Delta t}$ on the $\hat{Q}$ degree of freedom is merely to update it with the net number of electrons scattered into the fictitious leads, fixing $\hat{Q}_{t_{j+1}} - \hat{Q}_{t_j} = \Delta\hat{N}_p$, where $\Delta\hat{N}_p$ is the number of electrons absorbed by the probe in the event. This implies that $P_{Q_bQ_b}$ in Eq. (A14), which projects on the subspace with $Q = Q_b$, can be substituted by the electron-only operator that projects over scattered electronic states that satisfy $\hat{N}^{\text{out}}_p = \hat{N}^{\text{in}}_p + Q_b - Q_a$, where $\hat{N}^{\text{out}}_p$ is the number operator for fermions scattered into the probe, $\hat{N}^{\text{in}}_p$ is the number of electrons incident from the probe into the system at the beginning of the scattering event, and Q_a is the value of Q also at the beginning of the scattering event.

As anticipated just before the beginning of this subsection, the value of $\hat{N}^{\text{in}}_p$ on $|\phi^eQ_a\rangle$ is a function of Q_b, and should be chosen properly so as to compensate for a given excess probe charge Q_a at the beginning of a given scattering event. That way the fluctuations of the probe's excess charge Q will be minimum, although the precise choice does not affect the result as long as the resulting range of fluctuations of Q does not scale with measurement time t. As already discussed, for most cases the optimum choice is $N_p^{in}(Q) = g(Q)$, with

$$\begin{aligned} g(1) &= 2 \quad \text{(one electron in each lead of the probe)}, \\ g(0) &= g(-1) = 0, \end{aligned} \tag{A15}$$

which gives $Q \in [-1, 1]$, and a 3×3 $\overline{W}$ matrix.

To finish with the discussion of Eq. (A14) recall that $\hat{\chi_j} = e^{i \sum_k \lambda_k (\hat{N}_k^{\rm out} - \hat{N}_k^{\rm in})}$, and that a useful relation for the case of a single channel mode k in which the eigenvalues of $\hat{N}_k$ are zero and one is $e^{i\lambda_k \hat{N}_k} = 1 + (e^{i\lambda_k} - 1)\hat{N}_k$.

The whole Levitov-Lesovik formulation of FCS is well defined only in the long time limit. In such limit it is clear that expression (A14) is dominated by the biggest eigenvalues $\mu_{\rm max}$ of $\overline{W}$. All of its eigenvalues satisfy $|\mu| \leq 1$ for real values of $\vec{\lambda}$, so that those that are not close to 1 for small values of $\vec{\lambda}$ (around which we take derivatives to compute cumulants) will exponentiate to zero when $M \to \infty$. In all cases we examined only one eigenvalue $\mu_{\rm max}$ would not exponentiate to zero, although it can have finite degeneracy. In general, we have the following asymptotic property, valid for any degeneracy of $\mu_{\rm max}$,

$$\log \left[\chi(\vec{\lambda}; M) \right] = M \log \left[\mu_{\rm max} \right] + \mathcal{O}(1). \tag{A16}$$

We can define a new generating function $\chi_I(\vec{\lambda}) = \lim_{M\to\infty} \chi(\vec{\lambda}; M)/M$. It can be shown that this function generates the zero frequency limit or current cumulants, such as linear conductance and shot noise,

$$\langle\langle I_k(\omega = 0)^n \rangle\rangle = \frac{e^{n+1}|V|}{h} (-i)^n \, \partial^n_{\lambda_k} \log \chi_I \big|_{\vec{\lambda}=0}. \tag{A17}$$

We can identify

$$\chi_I(\vec{\lambda}) = \mu_{\rm max}(\vec{\lambda}). \tag{A18}$$

This is our final result. $\mu_{\rm max}$ is the eigenvalue of Eq. (A14) that equals 1 when all counting fields λ_k are taken to zero.

The generalization to multiple probes is very straightforward. Given the optimum choice of Eq. (A15), the solution of an $N-$probe setup will involve the diagonalization of an $3^N \times 3^N$ $\overline{W}$ matrix similar to Eq. (A14) where Q_n is changed to $\vec{Q}_n$, a vector of the N corresponding slave degrees of freedom.

A summary of the above results is given in Sec. III.

We have successfully compared the present method to scenarios where the previous techniques were applicable, obtaining identical results in all cases. Some simple examples are the FCS of a single channel wire with contact transmissions T, the case of a Mach-Zehnder interferometer or an NS junction, for which both this and the Langevin method [27] yield identical results for χ_I.

[1] I. Zutic, J. Fabian, and S. Das Sarma, Rev. Mod. Phys. **76**, 323 (2004).
[2] V. N. Golovach, A. Khaetskii, and D. Loss, Phys. Rev. Lett. **93**, 016601 (2004).
[3] J. R. Petta, A. C. Johnson, J. M. Taylor, E. A. Laird, A. Yacoby, M. D. Lukin, C. M. Marcus, M. P. Hanson, and A. C. Gossard, Science **309**, 2180 (2005).
[4] P. Recher, E. V. Sukhorukov, and D. Loss, Phys. Rev. Lett. **85**, 1962 (2000).
[5] P. G. Kwiat, K. Mattle, H. Weinfurter, A. Zeilinger, A. V. Sergienko, and Y. H. Shih, Phys. Rev. Lett. **75**, 4337 (1995).
[6] D. Bouwmeester, J. W. Pan, K. Mattle, M. Eibl, H. Weinfurter, and A. Zeilinger, Nature **390**, 575 (1997).
[7] A. Rauschenbeutel, G. Nogues, S. Osnaghi, P. Bertet, M. Brune, J. M. Raimond, and S. Haroche, Science **288**, 2024 (2000).
[8] MagiQ.
[9] D. Loss and D. P. DiVincenzo, Phys. Rev. A **57**, 120 (1998).
[10] R. Hanson, L. M. K. Vandersypen, L. H. W. van Beveren, J. M. Elzerman, I. T. Vink, and L. P. Kouwenhoven, Phys. Rev. B **70**, 241304 (2004).
[11] H. Ohno, Science **281**, 951 (1998).
[12] T. Koga, J. Nitta, and H. Takayanagi, Phys. Rev. Lett. **88**, 126601 (2002).
[13] Y. Kato, R. C. Myers, A. C. Gossard, and D. D. Awschalom, Nature **427**, 50 (2004).
[14] J. L. van Velsen, M. Kindermann, and C. W. J. Beenakker, Doga: Turk. J. Phys. **27**, 323 (2003).
[15] P. Samuelsson, E. V. Sukhorukov, and M. Büttiker, Doga: Turk. J. Phys. **27**, 481 (2003).
[16] C. W. J. Beenakker (2005), preprint archive cond-mat/0508488.
[17] E. Prada, F. Taddei, and R. Fazio, Phys. Rev. B **72**, 125333 (2005).
[18] F. Taddei, L. Faoro, E. Prada, and R. Fazio, New. J. Phys. **7**, 183 (2005).
[19] G. Burkard, D. Loss, and E. V. Sukhorukov, Phys. Rev. B **61**, 16303 (2000).
[20] P. Samuelsson, E. V. Sukhorukov, and M. Buttiker, Phys. Rev. B **70**, 115330 (2004).
[21] F. Taddei and R. Fazio, Phys. Rev. B **65**, 075317 (2002).
[22] J. C. Egues, G. Burkard, and D. Loss, Phys. Rev. Lett. **89**, 176401 (2002).
[23] G. Burkard and D. Loss, Phys. Rev. Lett. **91**, 087903 (2003).
[24] M. Buttiker, IBM J. Res. Dev. **32**, 63 (1988).
[25] M. Buttiker, Phys. Rev. Lett. **65**, 2901 (1990).
[26] Y. M. Blanter and M. Buttiker, Phys. Rep. **336**, 2 (2000).
[27] C. W. J. Beenakker, Phys. Rev. B **46**, 12841 (1992).
[28] G. Kiesslich, P. Samuelsson, A. Wacker, and E. Schöll (2005), preprint archive cond-mat/0507403.
[29] P. W. Brouwer and C. W. J. Beenakker, Phys. Rev. B **55**, 4695 (1997).
[30] L. E. F. Foa Torres, H. M. Pastawski, and E. Medina, Europhysics Letters (in press) (2005), preprint archive cond-mat/0511360.
[31] C. Texier and M. Buttiker, Phys. Rev. B **62**, 7454 (2000).
[32] S. Oberholzer, E. Bieri, C. Schoenenberger, M. Gio-

vannini, and J. Faist (2005), preprint archive cond-mat/0510240.
[33] F. Marquardt and C. Bruder, Phys. Rev. B **70**, 125305 (2004).
[34] S. Pilgram, P. Samuelsson, H. Forster, and M. Buttiker (2005), preprint archive cond-mat/0512276.
[35] P. Recher, E. V. Sukhorukov, and D. Loss, Phys. Rev. B **63**, 165314 (2001).
[36] J. B. Miller, D. M. Zumbuhl, C. M. Marcus, Y. B. Lyanda-Geller, D. Goldhaber-Gordon, K. Campman, and A. C. Gossard, Phys. Rev. Lett. **90**, 076807 (2003).
[37] P. Samuelsson, E. V. Sukhorukov, and M. Buttiker, Phys. Rev. Lett. **91**, 157002 (2003).
[38] B. Michaelis and C. W. J. Beenakker (2005), preprint archive cond-mat/0512465.
[39] M. J. M. deJong and C. W. J. Beenakker, Physica A **230**, 219 (1996).
[40] S. A. vanLangen and M. Buttiker, Phys. Rev. B **56**, R1680 (1997).
[41] V. S. W. Chung, P. Samuelsson, and M. Buttiker, Phys. Rev. B **72**, 125320 (2005).
[42] T. Martin and R. Landauer, Phys. Rev. B **45**, 1742 (1992).
[43] A. Shelankov and J. Rammer, Europhys. Lett. **63**, 485 (2003).
[44] Y. V. Nazarov and D. A. Bagrets, Phys. Rev. Lett. **88**, 196801 (2002).
[45] The shot noise normalized to e^3V/h is in fact the Fano factor since the total current is $I_{R_1} = e^2|V|T_B/h$
[46] Note the difference with the notation in [26]. When there is time reversal symmetry both choices are equivalent.